Scripta Materialia 271 (2026) 117050

Contents lists available at ScienceDirect

Scripta Materialia

journal homepage: www.journals.elsevier.com/scripta-materialia

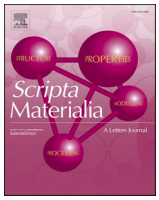

The triple junction line orientation distribution in polycrystals

Eileen L. Hung, Zipeng Xu, Gregory S. Rohrer [1,*]

Department of Materials Science and Engineering, Carnegie Mellon University, Pittsburgh, PA 15213, USA

ARTICLE INFO

Keywords:
Grain boundary
Triple line, microstructure

ABSTRACT

Two-dimensional triple line orientation distributions are calculated from three-dimensional experimental data for $SrTiO_3$, Ni, MgO, and 8 % Y_2O_3-stabilized ZrO_2. In the three cases where the triple line orientation distribution shows texture, it is consistent with the direction along which the most common grain boundary planes intersect, indicating that the triple line orientation distribution is determined by the grain boundary plane distribution. The majority of grain boundaries connected to two coherent twin boundaries in Ni had the symmetric $(1\bar{1}4)$ orientation, a boundary thought to have very low mobility. Boundaries with the symmetric $(\bar{2}21)$ orientation, reported to be more mobile, were not detected.

Triple lines are defects in polycrystals that occur at the intersection of three grain boundaries, as depicted in Fig. 1. While triple lines interact with a range of defects including segregated solute [1–3], grain boundary disconnections [4], and can serve as nucleation sites for precipitates [5] and new grains [6], they remain one of the least studied defects in crystals. In particular, with the exception of a few examples [7–10], little is known about their crystallographic distributions. This is likely because of their complexity. As concluded by Hardy and Field [7, 8], triple lines have 11 macroscopic crystallographic degrees of freedom. As a result, characterization of their distribution over all of these parameters would require amounts of data that appears unobtainable. Even when Hardy and Field [8] constrained this problem by assuming that one of the three grain boundaries was a twin, there remain six independent parameters and characterization of the distribution is challenging. Johnson and Schuh [9] considered only the grain boundary misorientations, similarly reducing the problem to six parameters. Saylor et al. [10] presented a much less complex two parameter triple line distribution. This distribution can be computed from three-dimensional orientation data that can now be obtained routinely by three-dimensional EBSD [11–13] or X-ray microscopy [14].

This letter has three purposes. The first is to provide a more detailed description of this two-parameter triple line orientation distribution than provided previously [10]. The second is to calculate and compare the distributions of four materials to better understand the origin of anisotropic triple junction line orientation distributions. The third purpose is to identify triple junctions in Ni comprised of two coherent twin boundaries (60°/[111]|(111)) to compare the distribution to predictions recently made about grain boundary migration via the disconnection mechanism [15].

We define the 11 triple line parameters in the following way. The first six parameters are two pairs of Euler angle triplets that define the misorientations of two of the three grain boundaries (the third misorientation is a dependent parameter) [16]. The next two parameters describe the unit vector that defines the orientation of the triple line in the crystal frame of reference. This line constrains the orientations of the three grain boundary planes because their normal vectors must be perpendicular to the triple line. Therefore, each of the three normal vectors has only one degree of freedom, completing the set of 11 parameters. To simplify this parameterization, we assume that the triple line orientation in the crystal reference frame is the essential defining characteristic of the defect. This simplification defines the defect as a two-parameter quantity, making its measurement relatively accessible.

Using the two-parameter description proposed above, the orientation distribution of triple lines in the crystal reference frame, $\tau(\mathbf{n})$, is calculated in the following way:

$$\tau(\boldsymbol{n}) = \frac{1}{m}\sum_{i=1}^{N}\sum_{j=1}^{3}\sum_{k=1}^{P} C_k g_j \boldsymbol{n}'_i l_i$$

In this expression, N is the number of observed triple lines, P is the number of proper symmetry operators in the crystal's point group, C_k are the proper symmetry operators (3 × 3 matrices), g_j is the 3 × 3

* Corresponding author.
E-mail address: gr20@andrew.cmu.edu (G.S. Rohrer).

[1] Gregory Rohrer was an Editor of the journal during the review period of the article. To avoid a conflict of interest, Gregory Rohrer was blinded to the record and another editor processed this manuscript.

https://doi.org/10.1016/j.scriptamat.2025.117050
Received 19 September 2025; Received in revised form 7 October 2025; Accepted 10 October 2025

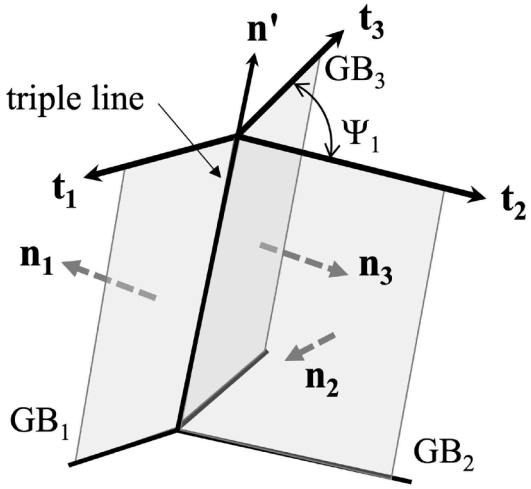

Fig. 1. The triple line geometry. The triple line direction is defined by the intersection of three grain boundaries (GB_i) with normal vectors ($\mathbf{n_i}$) and tangent lines in the plane of intersection ($\mathbf{t_i}$). One of the dihedral angles (Ψ_1) is also illustrated.

orientation matrix of the j^{th} crystal, $\mathbf{n}'$ is a unit vector in the sample reference frame in the direction of the triple line, and $l = |\mathbf{n}|$. The parameter m is a normalization factor discussed below. The data here were all derived from serial sectioning experiments with fixed distances between adjacent layers, yielding triple lines between these layers with nearly the same lengths. Thus, in the current analysis, the length of each line is approximated to be $|l_i| = 1$.

In the calculation, we parameterize the triple line orientations by two spherical angles (polar, θ, and azimuthal, ϕ) and classify the vectors into equal area discrete bins in the domain $0 \leq \cos\theta \leq 1$ and $0 \leq \phi \leq 2\pi$, using the scheme described in reference [17]. In this letter, the data has been discretized into nine bins per $\pi/2$. This distribution is normalized by the factor m, which is the average length per discrete bin, so that the results are in units of multiples of a random distribution (MRD) which in this case can be interpreted as relative length. To plot the distribution in the fundamental zone of the crystal, we sample the distribution at discrete orientations smaller than the bin size. Here we use previously described three-dimensional microstructure data for $SrTiO_3$ [18], Ni [12], MgO [10], and 8 % Y_2O_3 stabilized ZrO_2 (YSZ) [19]. These data were selected because they span four common metal and ceramic crystal structures and portions of the data are shown in Fig. 2. Using the same data, we also compute the grain boundary plane distribution (GBPD) in the crystal reference frame, $\lambda(\mathbf{n})$, a distribution defined previously [17]. While the grain boundary plane orientation distributions were included in the earlier reports [10,12,18,19], there is an important difference between the earlier distributions and the ones presented here. The previously reported distributions were computed from the complete set of grain boundary data. The grain boundary plane orientation distributions presented here were computed from only the segments of the boundaries that are attached to the triple junction. The data [20] and code (calc_TL_GBP_dist) [21] used for the calculations are available in publicly accessible repositories.

The computed triple junction line orientation distribution (TJLOD) can depend on the amount of data available. The number of triple lines in each data set is presented in Table 1. To examine how the distribution converges with the quantity of data, the orientation distribution of triple lines, $\tau(\mathbf{n})$, and grain boundary planes, $\lambda(\mathbf{n})$, were computed using different quantities of data. The computed distributions, illustrated in Fig. S1 and Fig. S2, show that the shapes of both distributions are approximately constant with 10,000 or more junctions. The extreme values of the distributions (see Fig. 2E) also stabilize after 10,000 or more junctions.

The triple junction line orientation distributions of $SrTiO_3$, Ni, MgO, and YSZ are shown in Fig. 3. Three of the distributions ($SrTiO_3$, Ni, and MgO) show texture in the sense that there are preferred line orientation directions, [110] for Ni and [100] for $SrTiO_3$ and MgO. The variations in the distribution for YSZ are ± 0.02 MRD. Such variations also result from computing the distribution from different subsets of the data (see Fig. 2E) and are considered insignificant. In other words, YSZ provides an example of a material with no texture in the triple line directions.

One hypothesis for the observed triple line distributions is that the triple line energy depends on orientation and the triple line arranges itself preferentially along the lowest energy directions, creating an anisotropic distribution [22]. Simulations have shown that triple

Table 1
Summary of data characteristics.

Material	Crystal Structure	Number of triple junctions	File name in archive	Description
$SrTiO_3$	Perovskite	25,673	triples_SrTiO3.txt	[18]
Ni	FCC	71,013	triples_Ni.txt	[12]
MgO	Rock Salt	19,094	triples_MgO.txt	[10]
8YSZ	Fluorite	87,237	triples_ZrO2.txt	[19]

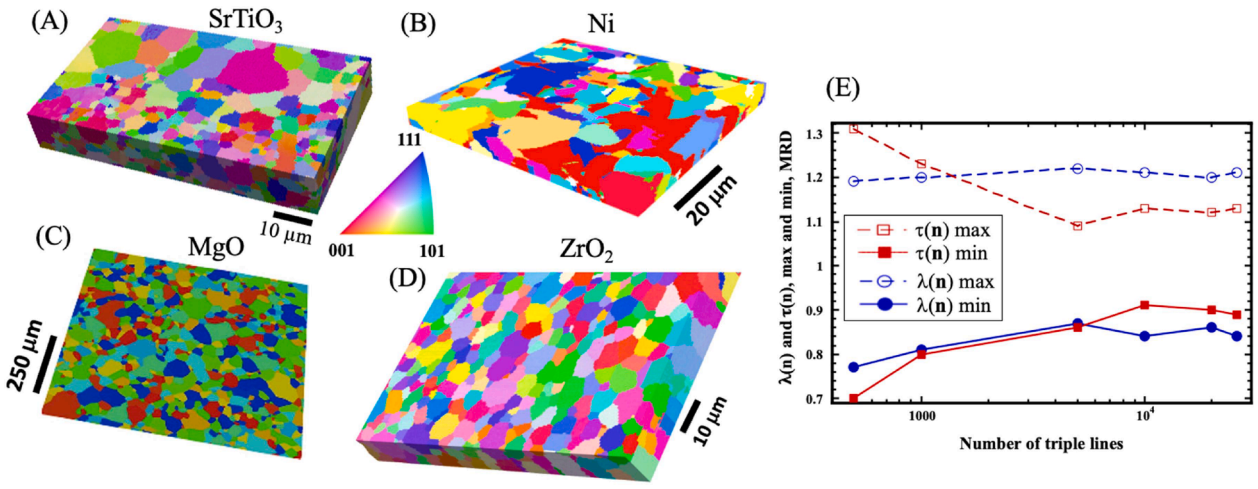

Fig. 2. Examples of the three-dimensional microstructure data and convergence of the distribution. The grains in A-D are colored by orientation with reference to vertical direction using the inset color key. Portion of the data for (A) $SrTiO_3$,(B) Ni, (C) MgO, and (D) ZrO_2. (E) The extreme values of the distributions shown in Fig. S1 ($\tau(\mathbf{n})$) and Fig. S2 ($\lambda(\mathbf{n})$) computed using different numbers of triple junctions.

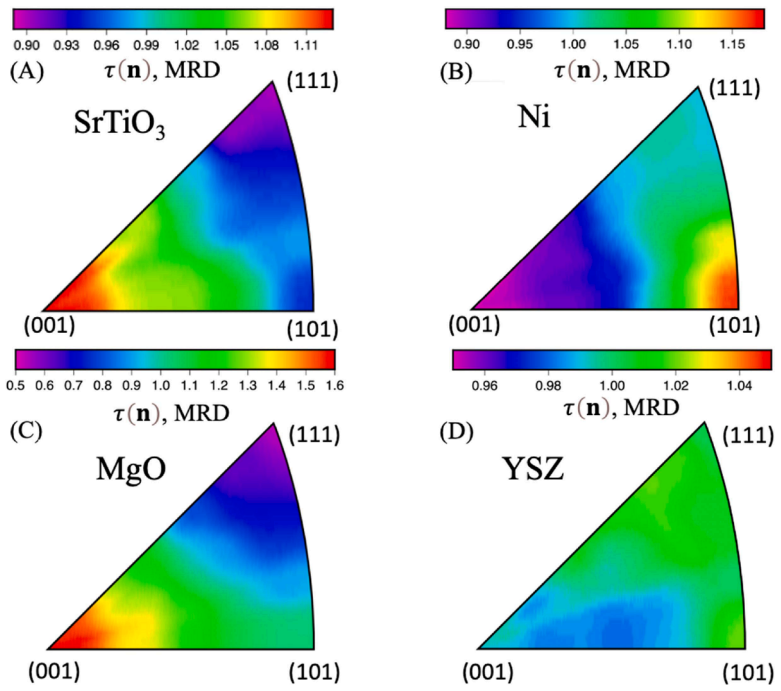

Fig. 3. Triple junction line orientation distributions. The triple junction line orientation distributions are plotted in stereographic projection in the crystal reference frame for (A) $SrTiO_3$, (B) Ni, (C) MgO, and (D) ZrO_2.

junctions have an excess energy and that it is negative [23,24]. The energy is negative because the triple junction has more degrees of freedom for energetic relaxation than the grain boundaries it replaces. In metals, the triple junction energy is on the order of 1/12th of the energy of a dislocation ($\approx -10^{-10}$ J/m) [24]. The excess energy of the junction can be shown formally to affect the equilibrium of the grain boundaries at the junction [25], but the magnitude of the energy could render this effect negligible. Because nothing is currently known about the anisotropy of the line energy, it is not possible to quantitatively test this hypothesis. From a qualitative viewpoint, we note that for Ni, [110] is the closest packed line direction (this is the slip direction), so this is certainly a reasonable choice for the lowest energy direction. The [110] direction also corresponds to the maximum in the TJLOD, consistent with the hypothesis. However, [110] is also the closest packed (and slip)

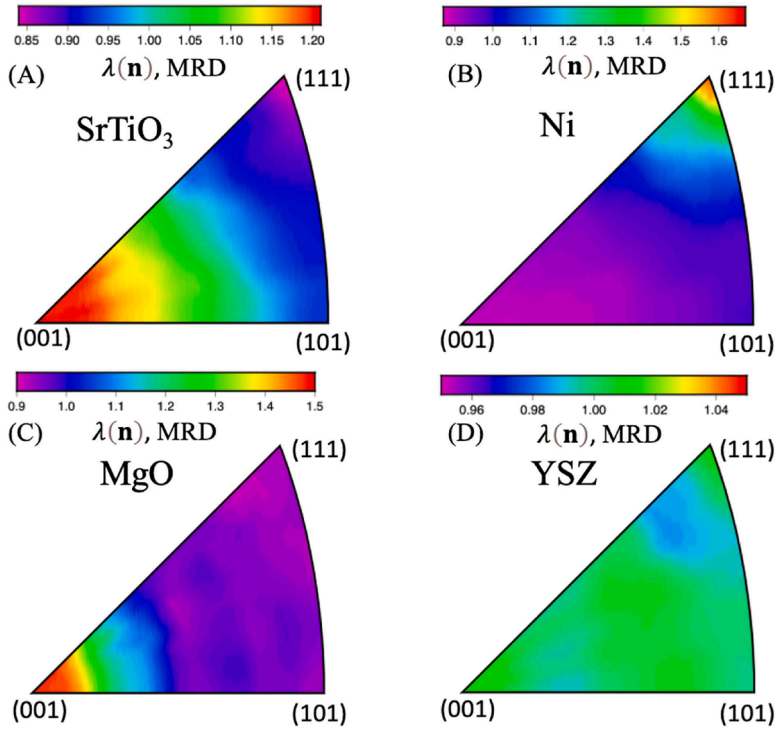

Fig. 4. Grain boundary plane orientation distributions. The distributions are plotted in stereographic projection in the crystal reference frame for (A) $SrTiO_3$, (B) Ni, (C) MgO, and (D) ZrO_2.

direction in perovskite structured $SrTiO_3$, rock salt structured MgO, and fluorite structured YSZ, where is does not correspond to a maximum in the TJLOD. Therefore, if one assumes that the low energy triple junction direction in a polycrystal is predicted by the closest packed slip direction, the bulk of the results do not support the hypothesis that the triple lines are distributed along low energy directions.

An alternate hypothesis is that the triple line directions are subordinate to the grain boundary plane orientations. For example, in his 2005 paper, Morawiec [25] concluded that complex interactions between the junction and connected microstructural elements "… puts emphasis on seeing a junction through the prism of attributes of adjacent boundaries." It has been found that grain boundary plane orientations do reflect the grain boundary energy anisotropy and maxima in the distribution are found at the lowest energy orientations [26]. Because some grain boundary plane orientations are preferred, there will also be preferred directions. Whenever two of the preferred grain boundary plane orientations meet at a junction, the line orientation direction must be the line of intersection, which is the direction that is mutually perpendicular to the two grain boundary normals. The grain boundary plane orientation distributions are shown in Fig. 4. For $SrTiO_3$, the preferred grain boundary plane orientation is (100) (see Fig. 4A). The intersection of two {100} oriented planes is the [100] direction, which is the maximum in the TJLOD (see Fig. 3A). The same is true for MgO. Furthermore, note that the maximum at the (100) orientation in the GBPD for MgO (see Fig. 4C) is greater than for $SrTiO_3$ (see Fig. 4A) and the corresponding maximum on the TJLOD of MgO (see Fig. 3C) is larger than for $SrTiO_3$ (see Fig. 3A). If the TJLOD is dictated by the orientation of the intersecting planes, then one would expect that more (100) planes would increase the number of [100] oriented triple junctions. For the case of Ni, the most common plane is (111) (see Fig. 4B) and the line of intersection between two {111} planes is the [110] orientation, corresponding the maximum in the TJLOD (see Fig. 3B). Finally, both the GBPD and TJLOD of YSZ are isotropic. We note that when the GBPD was computed from all of the grain boundary planes for YSZ, there was a very weak preference for (100) (1.1 MRD) [19], but this is not apparent when the distribution is computed from the boundaries adjacent to triple junctions. For all four examples, the TJLOD is consistent with the distribution that would arise from the intersection of the most common planes in the grain boundary plane orientation distribution.

In the remainder of this letter, we isolate and analyze a subset of the triple junctions in Ni that have two coherent twin boundaries and compare them to recent observations and simulations [15]. Ni contains many coherent twin boundaries (60°/[111]|(111)) meaning that we can find triple lines where two of these boundaries intersect. Approximately 200 of these triple lines were identified and filtered from the total data; their distribution is illustrated in Fig. 5A. Note that at this level of discretization, the maximum relative length is 14 MRD and this occurs when all of the observations fall into the same bin. Therefore, these 200 triple lines are, within experimental resolution, all aligned in the [110] direction as dictated by the geometry of the two coherent twin

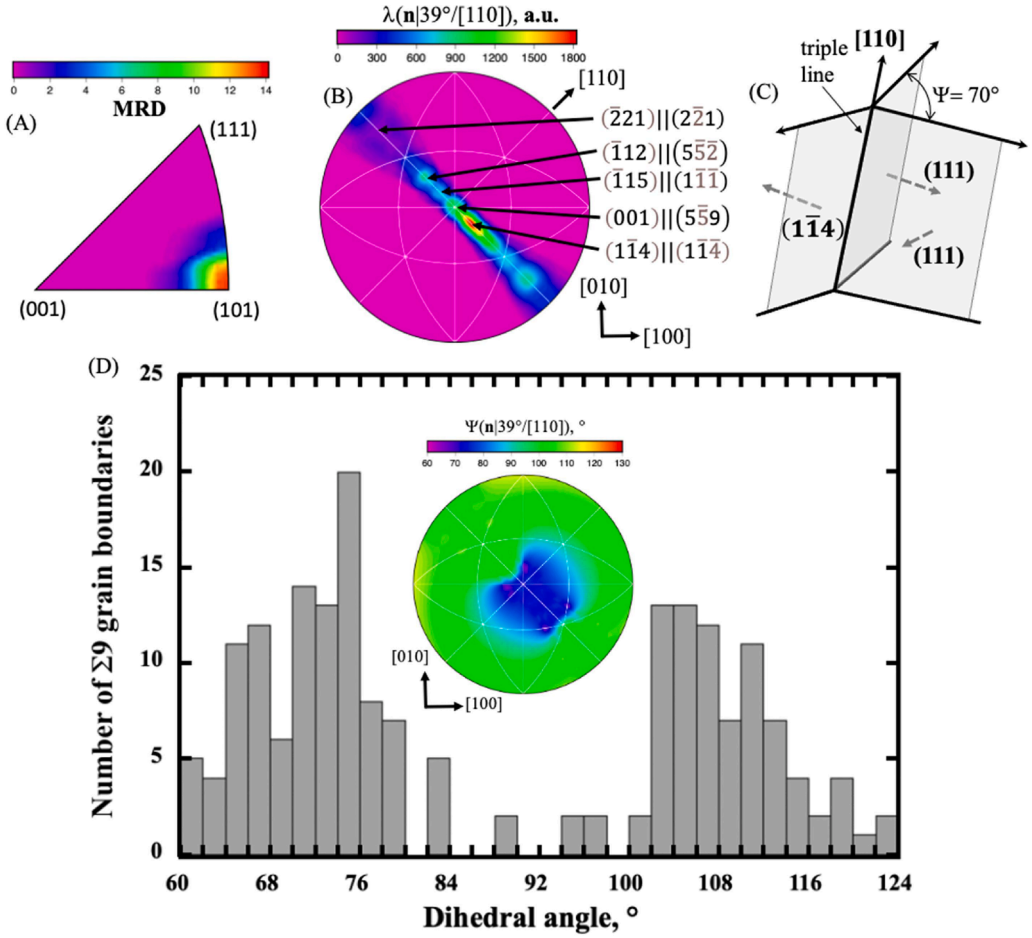

Fig. 5. Distribution of the triple junction line orientations, grain boundary plane orientations, and dihedral angles associated with triple junctions that include two coherent twin boundaries. (A) Triple line orientations. (B) The orientations of the grain boundaries at these junctions that are not twins. The boundary distribution is plotted with arbitrary units (a.u.). (C) Schematic diagram of the most common of these triple junctions defining the dihedral angle. (D) Histogram of dihedral angles. The inset shows the dihedral angle distribution plotted on a stereographic projection, illustrating that the lowest dihedral angles are concentrated near the $(1\bar{1}4)$ orientation.

boundaries.

For triple lines with two 60°/[111]|(111) twin boundaries, the third grain boundary is always 38.9°/[110] (Σ9) [16]. Furthermore, because the triple line is defined to be the intersection of two {111} planes (a ⟨110⟩ direction), the only remaining degree of freedom is the rotation of the grain boundary plane orientation around the triple line. Therefore, it must be a tilt grain boundary (the grain boundary plane normal is perpendicular to the misorientation axis). When we plot the relative areas of the 38.9°/[110] boundaries at these junctions (see Fig. 5B), there are only boundaries along the zone of tilts with the maximum at the orientation of the $(1\bar{1}4)$ symmetric tilt grain boundary. This triple junction is illustrated schematically in Fig. 5C. There are also three pairs of smaller local maxima indicating the presence of a smaller number of asymmetric tilt boundaries. The grain boundary planes for these boundaries are, from left to right, $(\bar{1}12)\|(5\bar{5}2)$, $(\bar{1}15)\|(1\bar{1}1)$, and $(100)\parallel(5\bar{5}9)$. Finally. We note that there is a second possibility for a symmetric tilt grain boundary at $(\bar{2}21)$, but there are no boundaries in this subset of junctions with that orientation.

The distribution of grain boundary dihedral angles for the 38.9°/[110] boundaries is plotted in Fig. 5D There are two noteworthy features of this distribution. The first is that nearly all of the angles are <120° This is because the twin boundaries have the minimum grain boundary energy in Ni [12,27] and the dihedral angle must shrink to stabilize the third higher energy boundary. The second feature is that the distribution is bimodal, with one maximum at about 74° and another at about 104°. When we compare this to the distribution of angles with orientation of the grain boundary plane (see Fig. 5D) we see that the symmetric $(1\bar{1}4)$ and the asymmetric $(100)\parallel(5\bar{5}9)$ have the lowest dihedral angles and the other asymmetric tilt boundaries have the larger dihedral angles. While this can be qualitatively associated with the relative energies of the boundaries through Young's equation, it should be recognized that the coherent twin boundaries are singular. For this reason, the torques terms, which are not known quantitatively, might be influential, if not dominant, for determining the dihedral angles at these junctions.

These particular triple junctions in Ni are of interest based on a recent prediction regarding disconnection theory. Xu et al. [15] demonstrated using simulations and experiments on thin films that triple lines of this type consisting of two coherent twins and a 38.9°/[110]|$(\bar{2}21)$ boundary migrate readily and those coupled with a 38.9°/[110]|$(1\bar{1}4)$ boundary are stagnant. The rational for this involves the character of the disconnections needed for the motion of all three boundaries. For the mobile junctions, the flux of disconnections to the triple line balances and there is no accumulation of residual stress associated with migration, while the opposite is true for the static junctions. While our data contain many of the junctions predicted to be static, we never observe any of the junctions that are predicted to be mobile. This could be interpreted as being consistent with the prediction if one assumes that the mobile junctions migrate so quickly they annihilate soon after they are formed and that is the reason they are not observed. The static ones, on the other hand, have a much longer lifetime and that is why we observe them. However, because the mobile junctions are completely absent from the data, one has to be skeptical that they were ever present in the microstructure. One can hypothesize that if they form, the boundary rotates under the influence of the torque forces to the minimum energy position at the $(1\bar{1}4)$ orientation (the $(1\bar{1}4)$ boundary is thought to be about 20 % lower in energy than the $(\bar{2}21)$ boundary [27]). Some boundaries might become trapped at the local minima associated with the asymmetric tilt boundaries and account for the observed distribution in Fig. 5B

In summary, an analysis of triple junction line orientation distributions in four polycrystals shows that anisotropy is sometimes present and that this anisotropy is consistent with the hypothesis that the triple junction line orientation distribution is determined by the grain boundary plane orientation distribution. The most common triple line orientation occurs at the intersection of the most common grain boundary planes. When the types of grain boundaries in Ni connected to two coherent twin boundaries were analyzed, only $(1\bar{1}4)$ symmetric tilt grain boundaries, predicted to be low mobility, and a smaller number of asymmetric tilt grain boundaries where found. Symmetric tilt grain boundaries with the $(\bar{2}21)$ orientation, predicted to be highly mobile and to have a larger energy, were absent from the data, making it impossible to quantify their relative mobility.

CRediT authorship contribution statement

Eileen L. Hung: Writing – review & editing, Investigation. **Zipeng Xu:** Writing – review & editing, Software, Investigation. **Gregory S. Rohrer:** Writing – review & editing, Writing – original draft, Methodology, Investigation, Conceptualization.

Declaration of competing interest

The author Gregory S. Rohrer is Coordinating Editor for Scripta Materialia and was not involved in the editorial review or the decision to publish this article.

Acknowledgments

This work was supported by the National Science Foundation under DMREF Grant No. 2118945.

Supplementary materials

Supplementary material associated with this article can be found, in the online version, at doi:10.1016/j.scriptamat.2025.117050.

References

[1] A.K. Barnett, O. Hussein, M. Alghalayini, A. Hinojos, J.E. Nathaniel II, D.L. Medlin, K. Hattar, B.L. Boyce, F. Abdeljawad, Triple junction segregation dominates the stability of nanocrystalline alloys, Nano Lett. 24 (2024) 9627–9634, https://doi.org/10.1021/acs.nanolett.4c02395.
[2] P. Stender, Z. Balogh, G. Schmitz, Triple junction segregation in nanocrystalline multilayers, Phys. Rev. B 83 (2011), https://doi.org/10.1103/PhysRevB.83.121407.
[3] N. Tuchinda, C.A. Schuh, Triple junction solute segregation in Al-based polycrystals, Phys. Rev. Mater. 7 (2023), https://doi.org/10.1103/PhysRevMaterials.7.023601.
[4] S.L. Thomas, K.T. Chen, J. Han, P.K. Purohit, D.J. Srolovitz, Reconciling grain growth and shear-coupled grain boundary migration, Nat. Comm. 8 (2017) 1764, https://doi.org/10.1038/s41467-017-01889-3.
[5] A.L. Greer, Triple lines in nucleation, Scripta Mater. 62 (2010) 899–903, https://doi.org/10.1016/j.scriptamat.2010.01.051.
[6] B. Lin, Y. Jin, C.M. Hefferan, S.F. Li, J. Lind, R.M. Suter, M. Bernacki, N. Bozzolo, A. D. Rollett, G.S. Rohrer, Observation of annealing twin nucleation at triple lines in nickel during grain growth, Acta Mater. 99 (2015) 63–68, https://doi.org/10.1016/j.actamat.2015.07.041.
[7] G.B. Hardy, D.P. Field, The parameters and fundamental zones of Twin-dependent triple junction distributions, Metall. Mater. Trans. A 46A (2015) 2273–2284, https://doi.org/10.1007/s11661-015-2800-0.
[8] G.B. Hardy, D.P. Field, Reliability of twin-dependent triple junction distributions measured from a section plane, Acta Mater. 103 (2016) 809–822, https://doi.org/10.1016/j.actamat.2015.10.038.
[9] O.K. Johnson, C.A. Schuh, The uncorrelated triple junction distribution function: towards grain boundary network design, Acta Mater. 61 (2013) 2863–2873, https://doi.org/10.1016/j.actamat.2013.01.025.
[10] D.M. Saylor, A. Morawiec, G.S. Rohrer, Distribution and energies of grain boundaries in magnesia as a function of five degrees of freedom, J. Am. Ceram. Soc. 85 (2002) 3081–3083, https://doi.org/10.1111/j.1151-2916.2002.tb00583.x.
[11] S.J. Dillon, G.S. Rohrer, Characterization of the grain-boundary character and energy distributions of Yttria using automated serial sectioning and EBSD in the FIB, J. Am. Ceram. Soc. 92 (2009) 1580–1585, https://doi.org/10.1111/j.1551-2916.2009.03064.x.
[12] J. Li, S.J. Dillon, G.S. Rohrer, Relative grain boundary area and energy distributions in nickel, Acta Mater. 57 (2009) 4304–4311, https://doi.org/10.1016/j.actamat.2009.06.004.
[13] D.M. Saylor, A. Morawiec, G.S. Rohrer, Distribution of grain boundaries in magnesia as a function of five macroscopic parameters, Acta Mater. 51 (2003) 3663–3674, https://doi.org/10.1016/s1359-6454(03)00181-2.

[14] J.V. Bernier, R.M. Suter, A.D. Rollett, J.D. Almer, High-energy X-ray diffraction microscopy in materials science, Annu. Rev. Mater. Res. 50 (2020) 395–436, https://doi.org/10.1146/annurev-matsci-070616124125.
[15] M.J. Xu, K.T. Chen, F. Cao, L. Velasco, T.M. Kaufman, F. Ye, H. Hahn, J. Han, D. J. Srolovitz, X.Q. Pan, Disconnection-mediated Twin/Twin-junction migration in FCC metals, Acta Mater. 240 (2022), https://doi.org/10.1016/j.actamat.2022.118339.
[16] K. Miyazawa, Y. Iwasaki, K. Ito, Y. Ishida, Combination rule of Sigma values at triple junctions in cubic polycrystals, Acta Cryst. A 52 (1996) 787–796, https://doi.org/10.1107/s0108767396005934.
[17] G.S. Rohrer, D.M. Saylor, B. El Dasher, B.L. Adams, A.D. Rollett, P. Wynblatt, The distribution of internal interfaces in polycrystals, Z. Metallkd. 95 (2004) 197–214, https://doi.org/10.3139/ijmr-2004-0043.
[18] X.T. Zhong, M.N. Kelly, H.M. Miller, S.J. Dillon, G.S. Rohrer, Grain boundary curvatures in polycrystalline $SrTiO_3$: dependence on grain size, topology, and crystallography, J. Amer. Ceram. Soc. 102 (2019) 7003–7014, https://doi.org/10.1111/jace.16608.
[19] S.J. Dillon, Y.F. Shen, G.S. Rohrer, Grain boundary energies in yttria-stabilized zirconia, J. Am. Ceram. Soc. 105 (2022) 2925–2931, https://doi.org/10.1111/jace.18283.
[20] E.L. Hung, Z.P. Xu, G.S. Rohrer, Triple Junct. Line Orientat. Distrib. (2025). http://mimp.materials.cmu.edu/~gr20/Grain_Boundary_Data_Archive/TJLOD_project/TJLOD.html.
[21] G.S. Rohrer. calc_TL_GBP_dist, (2025), https://github.com/gr20cmu/gbXstallography/blob/main/calc_TL_GBP_dist.
[22] W.C. Carter, M. Baram, M. Drozdov, W.D. Kaplan, Four questions about triple lines, Scripta Mater. 62 (2010) 894–898, https://doi.org/10.1016/j.scriptamat.2010.02.027.
[23] S.G. Srinivasan, J.W. Cahn, H. Jónsson, G. Kalonji, Excess energy of grain-boundary trijunctions: an atomistic simulation study, Acta Mater. 47 (1999) 2821–2829, https://doi.org/10.1016/S1359-6454(99)00120-2.
[24] N. Tuchinda, C.A. Schuh, Triple junction excess energy in polycrystalline metals, Acta Mater. 279 (2024), https://doi.org/10.1016/j.actamat.2024.120274.
[25] A. Morawiec, On equilibrium conditions at junctions of anisotropic interfaces, J Mater. Sci. 40 (2005) 2803–2806, https://doi.org/10.1007/s10853-005-2411-z.
[26] G.S. Rohrer, Grain boundary energy anisotropy: a review, J. Mater. Sci. 46 (2011) 5881–5895, https://doi.org/10.1007/s10853-011-5677-3.
[27] D.L. Olmsted, S.M. Foiles, E.A. Holm, Survey of computed grain boundary properties in face-centered cubic metals: I. Grain boundary energy, Acta Mater. 57 (2009) 3694–3703, https://doi.org/10.1016/j.actamat.2009.04.007.

Supplemental Information for: The triple junction line orientation distribution in polycrystals

Eileen L. Hung, Zipeng Xu, and Gregory S. Rohrer

Department of Materials Science and Engineering, Carnegie Mellon University, Pittsburgh, PA 15213

Figures S1 and S2 summarize what happens when the triple junction line and grain boundary plane orientation distributions (TJLOD and GBPD) are computed using different numbers of triple junctions from the same data set for $SrTiO_3$. The distributions were computed using the first N triple junctions in the data, where N = 500, 1000, 5000, 10000, 20000, and 25673 (the complete set). The shapes of the TJLODs (see Fig. S1) and the GBPDs (see Fig. S2), as well as the extreme values of the distributions (see Fig. 2E) and are essentially constant after about 10000 junctions.

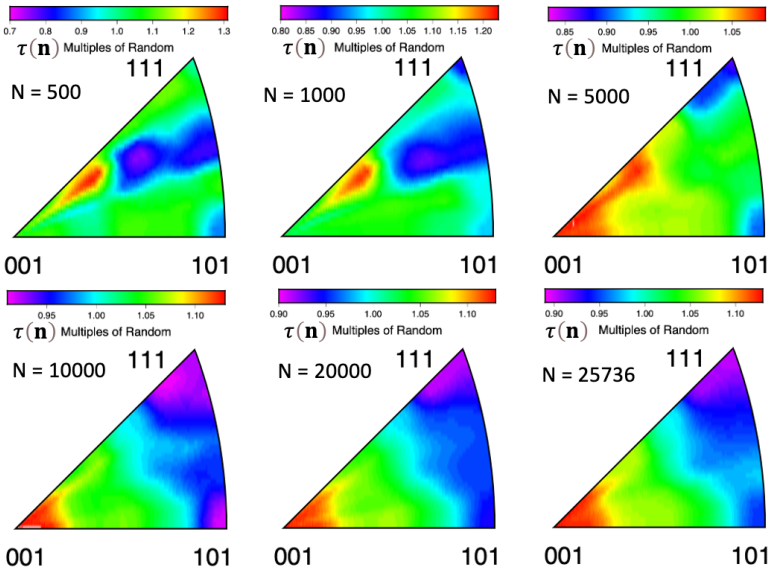

Figure S1. The triple junction line orientation distribution ($\tau(\mathbf{n})$) of $SrTiO_3$ computed using different numbers (N) of triple junctions.

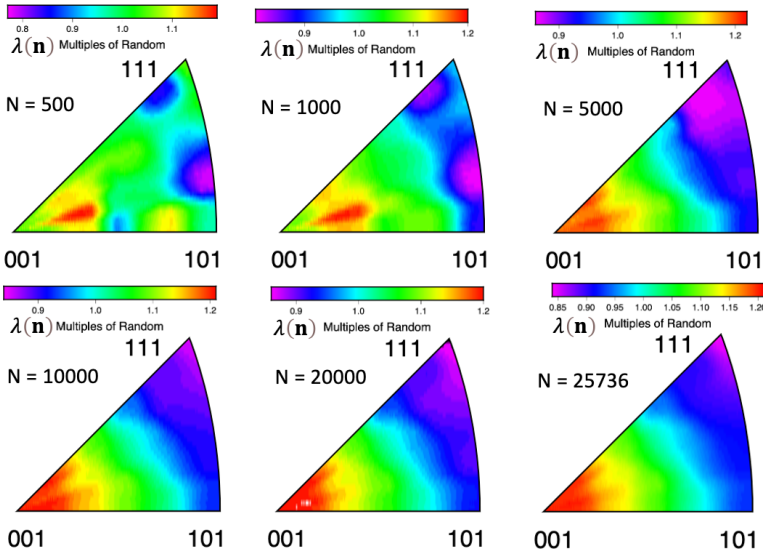

Figure S2. The grain boundary plane orientation distribution ($\lambda(\mathbf{n})$) of $SrTiO_3$ computed using different numbers (N) of triple junctions.